The Astrophysical Journal Letters, 943:L22 (6pp), 2023 February 1 https://doi.org/10.3847/2041-8213/acb157

New Constraints for Supernova Models from Presolar Silicon Carbide X Grains with Very High $^{26}Al/^{27}Al$ Ratios

Peter Hoppe[1], Jan Leitner[1,2], Marco Pignatari[3,4,5], and Sachiko Amari[6,7]
[1] Max Planck Institute for Chemistry, Hahn-Meitner-Weg 1, D-55128 Mainz, Germany; peter.hoppe@mpic.de
[2] Institute of Earth Sciences, Heidelberg University, Im Neuenheimer Feld 234-236, D-69120 Heidelberg, Germany
[3] Konkoly Observatory, Konkoly Thege Miklos ut 15-17, 1121, Budapest, Hungary
[4] E. A. Milne Centre for Astrophysics, University of Hull, HU6 7RX, Hull, UK
[5] NuGrid Collaboration, USA[8]
[6] McDonnell Center for the Space Sciences and Physics Department, Washington University, St. Louis, MO 63130, USA
[7] Geochemical Research Center, The University of Tokyo, Tokyo, 113-0033, Japan
Received 2022 December 5; revised 2023 January 9; accepted 2023 January 9; published 2023 February 1

Abstract

We report C, N, Mg-Al, Si, and S isotope data of six 1–3 μm-sized SiC grains of Type X from the Murchison CM2 chondrite, believed to have formed in the ejecta of core-collapse supernova (CCSN) explosions. Their C, N, and Si isotopic compositions are fully compatible with previously studied X grains. Magnesium is essentially monoisotopic ^{26}Mg which gives clear evidence for the decay of radioactive ^{26}Al. Inferred initial $^{26}Al/^{27}Al$ ratios are between 0.6 and 0.78 which is at the upper end of previously observed ratios of X grains. Contamination with terrestrial or solar system Al apparently is low or absent, which makes the X grains from this study particularly interesting and useful for a quantitative comparison of Al isotope data with predictions from supernova models. The consistently high $^{26}Al/^{27}Al$ ratios observed here may suggest that the lower $^{26}Al/^{27}Al$ ratios of many X grains from the literature are the result of significant Al contamination and in part also of an improper quantification of ^{26}Al. The real dispersion of $^{26}Al/^{27}Al$ ratios in X grains needs to be explored by future studies. The high observed $^{26}Al/^{27}Al$ ratios in this work provide a crucial constraint for the production of ^{26}Al in CCSN models. We explored different CCSN models, including both "classical" and H ingestion CCSN models. It is found that the classical models cannot account for the high $^{26}Al/^{27}Al$ ratios observed here; in contrast, H ingestion models are able to reproduce the $^{26}Al/^{27}Al$ ratios along with C, N, and Si isotopic ratios reasonably well.

Unified Astronomy Thesaurus concepts: Circumstellar matter (241); Meteorites (1038); Nucleosynthesis (1131); Supernovae (1668)

1. Introduction

Primitive solar system materials, e.g., undifferentiated meteorites, contain small quantities of so-called presolar grains that formed in the winds of evolved stars and in the ejecta of stellar explosions (Zinner 2014; Nittler & Ciesla 2016). These pristine dust grains represent a sample of stardust that can be analyzed in terrestrial laboratories in great detail. Presolar grains can be identified in primitive solar system materials because they show highly anomalous isotopic compositions, the nucleosynthetic fingerprints of their parent stars. Laboratory analyses of presolar grains have provided a wealth of information on stellar nucleosynthesis and evolution, mixing in supernova (SN) ejecta, dust formation in stellar environments, and the inventory of stars that contributed dust to our solar system.

Silicon carbide (SiC) is the second-most abundant presolar mineral after silicates, but best characterized. It was identified more than 30 yr ago (Bernatowicz et al. 1987) because it is tagged with noble gases of anomalous isotopic compositions (Lewis et al. 1994). Later studies of bulk samples and of individual grains showed that the major elements C and Si, and many minor elements contained in presolar SiC have highly anomalous isotopic compositions as well. Based on the isotopic compositions of C, N, and Si of individual grains, presolar SiC is divided into distinct populations (Zinner 2014): mainstream grains, which account for about 80%–90% of all grains, and the minor types AB, C, X, Y, Z, and (putative) nova grains. Mainstream grains are believed to originate from low-mass (1.5–3 $M_{\odot}$) asymptotic giant branch (AGB) stars of about solar or super-solar metallicity (e.g., Lugaro et al. 2003, 2018; Palmerini et al. 2021 and references therein). Core-collapse supernovae (CCSNe) contributed to the population of presolar SiC grains as well. Signatures of SN nucleosynthesis are seen in the isotope patterns of the minor Type C and X grains (Amari et al. 1992; Hoppe et al. 1996; Nittler et al. 1996; Gyngard et al. 2010), and in a significant fraction of Type AB (Liu et al. 2017; Hoppe et al. 2019) and (putative) nova grains (Nittler & Hoppe 2005; Liu et al. 2017; Hoppe et al. 2018).

Of particular interest are the SN-derived X grains. X grains account for about 1%–2% of all presolar SiC grains and were the first identified presolar SiC grains with an SN origin (Amari et al. 1992). X grains exhibit "exotic" isotopic signatures of many elements, and it is general consensus that these grains formed in the ejecta of CCSN explosions (e.g., Amari et al. 1992; Hoppe et al. 1996; Nittler et al. 1996; Hoppe et al. 2000; Lin et al. 2002; Nittler & Alexander 2003; Besmehn & Hoppe 2003; Hoppe et al. 2010; Lin et al. 2010; Xu et al. 2015; Liu et al. 2018). X grains exhibit a wide range of $^{12}C/^{13}C$ ratios from 7 to 10,000, but most have higher $^{12}C/^{13}C$ ratios

[8] http://www.nugridstars.org

Table 1
C, N, Al, Si, and S Isotopic Compositions

Grain	$^{12}C/^{13}C$	$^{14}N/^{15}N$	$^{26}Al/^{27}Al$	Mg/Al[a]	$\delta^{29}Si$ (‰)[b]	$\delta^{30}Si$ (‰)[b]	$\delta^{34}S$ (‰)[c]
KJF-X1	612 ± 8	37.5 ± 0.1	0.665 ± 0.004	0.91 ± 0.06	-304 ± 2	-588 ± 2	-25 ± 60
KJF-X2	738 ± 11	78.5 ± 0.6	0.599 ± 0.006	0.65 ± 0.18	-320 ± 2	-446 ± 2	-167 ± 100
KJF-X3	200 ± 2	64.9 ± 0.3	0.665 ± 0.004	0.75 ± 0.10	-305 ± 3	-535 ± 4	-16 ± 41
KJF-X4	341 ± 3	118.6 ± 0.8	0.655 ± 0.007	<0.50[d]	-631 ± 1	-376 ± 2	-41 ± 53
KJF-X5	246 ± 2	60.2 ± 0.2	0.778 ± 0.003	0.79 ± 0.08	-260 ± 2	-477 ± 2	-178 ± 109
KJF-X6	462 ± 4	43.6 ± 0.1	0.666 ± 0.004	0.93 ± 0.05	-312 ± 2	-544 ± 2	67 ± 64
X4[e]	2525 ± 143	12.6 ± 0.1	0.605 ± 0.035		-363 ± 2	-529 ± 2	n.m.[g]
Bonanza[f]	190 ± 1	27.6 ± 0.1	0.598 ± 0.001		-292 ± 4	-448 ± 4	-14 ± 4

Note. Six SiC X grains are from Murchison separate KJF (this study) and two X grains with high $^{26}Al/^{27}Al$ are from the literature. [a] Measured by SEM-EDX. [b] $\delta^{x}Si = [(^{x}Si/^{28}Si)_{grain}/(^{x}Si/^{28}Si)_{solar}—1] \times 1000$, x = 29, 30. [c] $\delta^{34}S = [(^{34}S/^{32}S)_{grain}/(^{34}S/^{32}S)_{solar}—1] \times 1000$. [d] 2σ upper limit. [e] Amari et al. (1992). [f] Gyngard et al. (2018). [g] n.m.: not measured.

than solar (89). They have $^{14}N/^{15}N$ ratios between 7 and 400, i.e., all are enriched in ^{15}N relative to the solar $^{14}N/^{15}N$ ratio of 440 (Marty et al. 2011). Silicon is isotopically light with enrichments in ^{28}Si up to a factor of five. Other important signatures of X grains are high abundances of radiogenic ^{26}Mg from the decay of radioactive ^{26}Al (half-life: 716 kyr), with initial $^{26}Al/^{27}Al$ ratios between 0.01 and ~0.6, and the presence of radiogenic ^{44}Ca from the decay of radioactive ^{44}Ti (half-life: 60 yr) in some grains. Liu et al. (2021) pointed out that measured C, N, and Al isotopic compositions of presolar SiC might be compromised by contamination, and that true compositions could be more extreme; a similar conclusion was made by Groopman et al. (2015) for initial $^{26}Al/^{27}Al$ ratios. This is an important aspect when the isotope data of presolar grains are quantitatively compared with stellar model predictions.

Here, we report on a search for new SiC X grains by NanoSIMS ion imaging and subsequent high spatial resolution measurements of C, N, Mg-Al, Si, and S isotopic compositions of six micrometer-sized X grains from the Murchison CM2 meteorite. Specific care was taken to exclude contamination on or around grains and on the determination of the Mg-Al relative sensitivity factor for NanoSIMS analyses, needed to infer initial $^{26}Al/^{27}Al$ ratios, to get unbiased isotopic compositions. The major goals of our study are (i) to explore to which extent $^{26}Al/^{27}Al$ data from previous studies of X grains might be biased, and (ii) to provide new constraints for SN models from $^{26}Al/^{27}Al$ data. For this purpose we will compare the multielement isotope data of X grains with predictions from a set of twelve SN models.

2. Experimental

Several hundred SiC grains from the Murchison separate KJF (median size: 1.86 μm; Amari et al. 1994), dispersed on a clean gold foil, were screened by C and Si ion imaging with the NanoSIMS ion probe at the Max Planck Institute for Chemistry to search for X grains. A focused Cs^+ primary ion beam (~4 pA, 200 nm) was rastered over 688 30×30 μm^2-sized areas on the gold foil and negative secondary ion images of ^{12}C, ^{13}C, ^{28}Si, ^{29}Si, and ^{30}Si were recorded in multicollection (256×256 pixels, 15,000–20,000 μs/pixel). Subsequently, six identified X grains (KJF-X1...6), 1–3 μm in size, were measured with a high spatial resolution for C, N, Si, S, and Mg-Al isotopic compositions (image sizes: 3×3 to 5×5 μm^2). We recorded in multicollection negative secondary ions of (i) ^{12}C, ^{13}C, ^{28}Si, ^{29}Si, and ^{30}Si and of (ii) ^{12}C, $^{12}C^{14}N$, $^{12}C^{15}N$, ^{32}S, and ^{34}S, using the Cs^+ ion source (~1 pA, 100 nm), followed by (iii) measurement of positive secondary ions of ^{24}Mg, ^{25}Mg, ^{26}Mg, ^{27}Al, and ^{28}Si, employing the Hyperion O^- primary ion source (~3 pA, 100 nm).

Initial $^{26}Al/^{27}Al$ ratios were calculated from $[^{26}Mg^+–^{24}Mg^+ \times (^{26}Mg^+/^{24}Mg^+)_{standard}]/^{27}Al^+ \times \varepsilon(Al^+/Mg^+)$. $\varepsilon(Al^+/Mg^+)$ is the relative sensitivity factor. It is defined as $(Al^+/Mg^+)_{measured}/(Al/Mg)_{true}$ and can be inferred from measurements on standards with known Al/Mg ratios. Here, we measured $\varepsilon(Al^+/Mg^+)$ on four different standards, a wafer of NIST SRM 611 glass (Al/Mg = 21.2), a flat, polished sample of Mahenge spinel (Al/Mg = 2.0), and fine-grained samples of NIST SRM 611 glass (0.3–0.8 μm) and Mahenge spinel (0.6–2.5 μm). Inferred $\varepsilon(Al^+/Mg^+)$ values are 0.76 ± 0.03 (NIST SRM 611 glass wafer), 0.79 ± 0.04 (flat, polished Mahenge spinel), 1.65 ± 0.19 (NIST SRM 611 grains), and 1.13 ± 0.03 (Mahenge spinel grains), respectively. These data show that the Al/Mg sensitivity factor depends strongly on sample topography, with 1.4 to 2.2 times higher values for micrometer- and submicrometer-sized grains. As the KJF SiC grains are of comparable size, we used the Al^+/Mg^+ sensitivity factor inferred from grains to calculate initial $^{26}Al/^{27}Al$ ratios. In previous studies of SiC grains by our group (Hoppe et al. 2010, 2012, 2018, 2019) we used a value of 1.56 for the Al^+/Mg^+ sensitivity factor, inferred from measurements on small spinel grains from the Murray meteorite (Hoppe et al. 2010). This value is between those inferred here for NIST SRM 611 grains and Mahenge spinel grains and we will use this value for consistency with our previous studies.

To follow up on the Al^+/Mg^+ sensitivity factor we have measured Mg/Al ratios of the six X grains by energy-dispersive X-ray (EDX) analysis with a Leo 1530 field emission scanning electron microscope (SEM) equipped with an Oxford Instruments X-Max 80 EDX detector (15 kV acceleration voltage, 90 s measurement time, quantification with Aztec 3.1). Uncertainties for the Mg/Al ratios are based on counting statistics, with relative errors from 5.4% to 28% (owed to Mg and Al concentration close to the detection limit).

3. Results

Among 964 identified presolar SiC grains are 831 mainstream grains (87%), 50 AB grains (5%), 77 Y and Z grains (8%), and six X grains (0.6%). The C, N, Al, Si, and S isotope data of the six X grains from this study and of the two X grains with the highest $^{26}Al/^{27}Al$ ratios from the literature (Amari

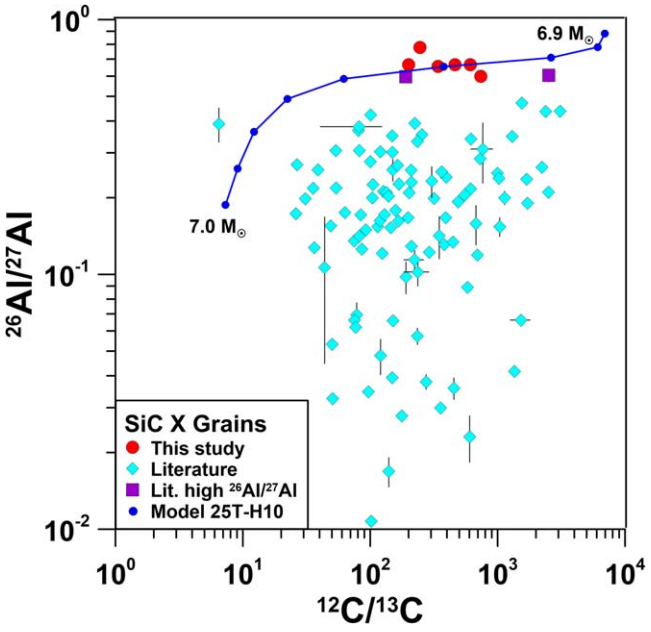

Figure 1. The $^{26}Al/^{27}Al$ and $^{12}C/^{13}C$ ratios of six SiC X grains from this study (red circles) along with data from the literature (light blue diamonds and purple squares; see a compilation of data in Stephan et al. 2021). Errors are 1σ. The C and Al data of grains from this study and two grains from the literature with $^{26}Al/^{27}Al$ ratios of ~0.6 (Amari et al. 1992 Gyngard et al. 2018) are well matched by SN model 25T-H10 of Pignatari et al. (2015) at mass coordinate 6.93–6.95 $M_\odot$ (the blue solid line which connects the nine data points from the model in this mass range).

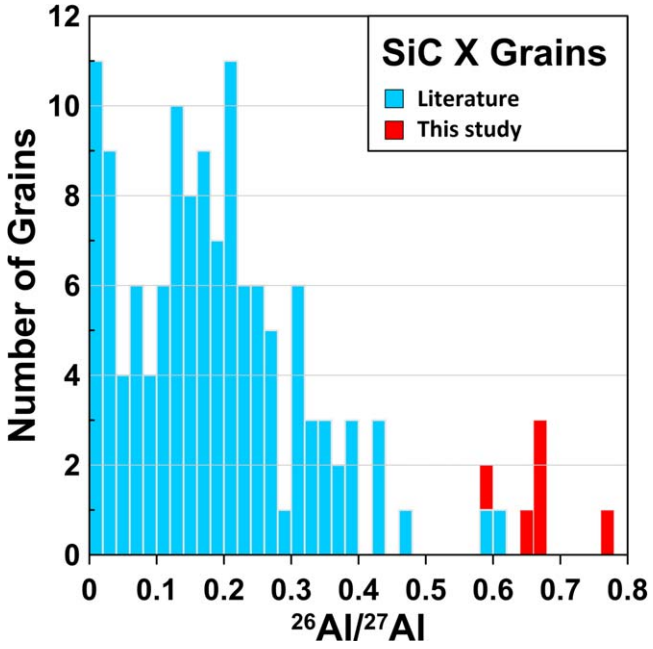

Figure 2. Histogram of initial $^{26}Al/^{27}Al$ ratios of six SiC X grains from this study (red) and of X grains from the literature (see a compilation of data in Stephan et al. 2021). Bin size is 0.02. All our data plot above $^{26}Al/^{27}Al > \sim 0.6$ while only ~2% of X grains from the literature fall in this range.

et al. 1992; Gyngard et al. 2018) are given in Table 1 and Figures 1 and 2. The X grains from this study have $^{12}C/^{13}C$ ratios between 200 and 738, i.e., higher-than-solar, $^{14}N/^{15}N$ ratios from 39 to 119, i.e., lower-than-solar, $^{29}Si/^{28}Si$ ratios of 0.37–0.74 x solar, and $^{30}Si/^{28}Si$ ratios of 0.41–0.62 x solar. Five X grains show lower-than-solar $^{34}S/^{32}S$ ratios, with ^{32}S enrichments of up to 18%, although statistically not significant. Depletions of heavy S isotopes are interpreted to be due to ^{32}Si decay (half-life: 153 yr; Pignatari et al. 2013); inferred initial $^{32}Si/^{28}Si$ ratios are $2–4 \times 10^{-5}$.

Magnesium is essentially monoisotopic ^{26}Mg in all X grains, which is clear evidence for the decay of radioactive ^{26}Al. Inferred initial $^{26}Al/^{27}Al$ ratios are between 0.60 and 0.78, which is at the upper end of literature data for X grains (Figures 1 and 2), suggesting only low levels of Al contamination. An example is shown in Figure 3 where positive secondary ion images of ^{24}Mg, ^{26}Mg, ^{27}Al, ^{28}Si, and $^{26}Mg/^{27}Al$ along with the SEM image of grain KJF-X5 are displayed.

Since Mg is essentially radiogenic ^{26}Mg, Mg/Al ratios measured by SEM-EDX are a good proxy for the initial $^{26}Al/^{27}Al$ ratios of X grains. Aluminum concentrations were determined to be 0.5–3.1 at%. Three grains (KJF-X1, KJF-X5, KJF-X6) have relatively high Al concentrations of >1 at% and Mg/Al ratios between 0.79 and 0.93; the three grains with lower Al concentration have Mg/Al ratios of 0.5 (KJF-X4, only 2σ upper limit determined because Mg was below detection limit), 0.65 (KJF-X2), and 0.75 (KJF-X3; Table 1). These ratios are relatively close to the $^{26}Al/^{27}Al$ ratios determined by NanoSIMS which supports the validity of the Al^+/Mg^+ sensitivity factor used here and implies that matrix effects are only moderate. Based on the SEM-EDX data and the range of observed Al^+/Mg^+ sensitivity factors of grain samples we estimate that $^{26}Al/^{27}Al$ ratios of X grains in this work have systematic uncertainties of 20%–30% (in addition to the errors reported in Table 1).

4. Discussion

The C, N, Si, and S isotopic data of our new X grains are fully compatible with those from the literature (Zinner 2014; Stephan et al. 2021). Initial $^{26}Al/^{27}Al$ ratios, on the other hand, are higher than those of most X grains (Figures 1, 2); only two X grains from the literature have comparably high whole-grain $^{26}Al/^{27}Al$ ratios of ~0.6 (Amari et al. 1992; Gyngard et al. 2018). At first glance this looks surprising but it was argued before that Mg-Al isotope measurements of many presolar SiC grains were strongly compromised by substantial contamination with Al of terrestrial or solar system origin (Groopman et al. 2015; Liu et al. 2021). This would lower inferred initial $^{26}Al/^{27}Al$ ratios. Inspection of ion images of our new X grains suggests little to no Al contamination on or around X grains (Figure 3). The high $^{26}Al/^{27}Al$ ratios of X grains reported here give thus further support to the view that the $^{26}Al/^{27}Al$ data of many X grains from the literature are too low. This makes a comprehensive comparison of X grain data from the literature with SN models difficult. We note that this would be true also for other types of presolar grains, e.g., SiC grains from AGB stars and graphites.

We have shown here that the Al^+/Mg^+ sensitivity factor of SIMS measurements is strongly dependent on sample topography. Often Mg-Al sensitivity factors are not given in the literature when $^{26}Al/^{27}Al$ ratios of presolar grains are reported. Some NanoSIMS studies (e.g., Lin et al. 2010; Liu et al. 2021), however, used values around 0.8, similar to the values we inferred for large, flat standard samples and about a factor of 2 lower than the value we inferred for submicrometer- and micrometer-sized grains. It is unlikely that the lower value is

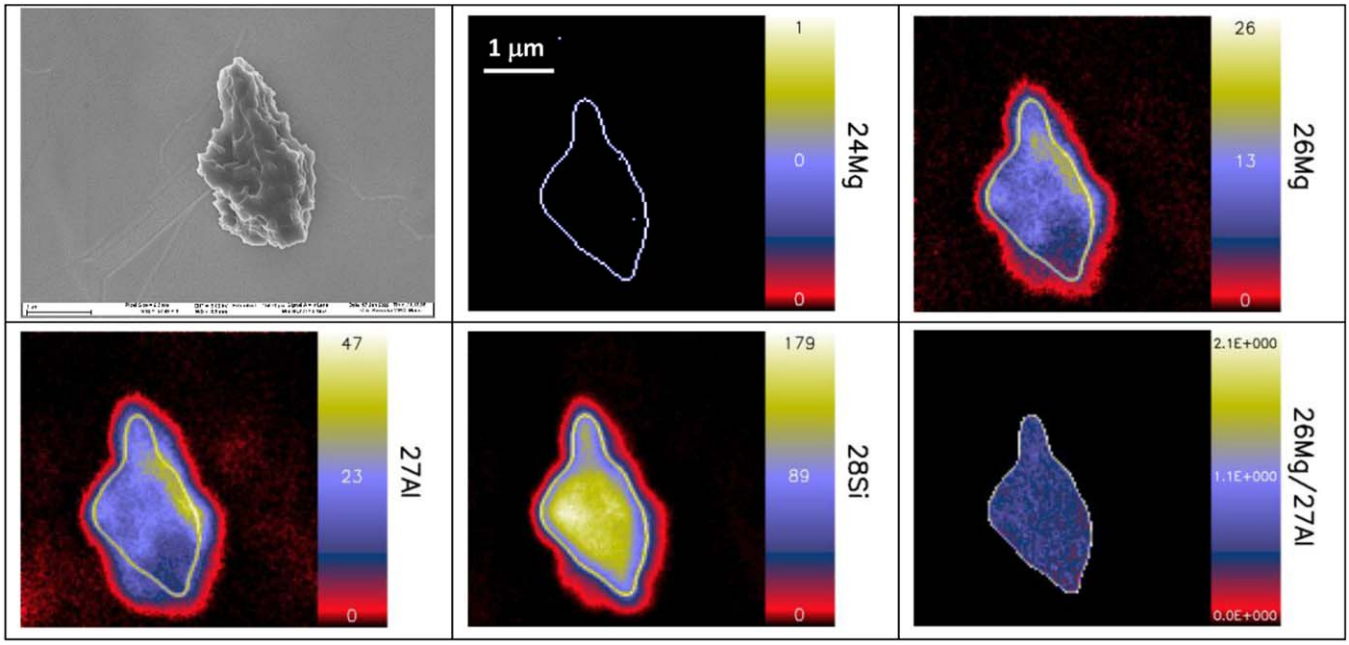

Figure 3. SEM image and NanoSIMS ion images of $^{24}Mg^+$, $^{26}Mg^+$, $^{27}Al^+$, $^{28}Si^+$, and $^{26}Mg^+/^{27}Al^+$ of SiC X grain KJF-X5. The scale bar shown in the $^{24}Mg^+$ image applies to all images. As it can be seen from the two Mg ion images in the upper row, Mg is essentially monoisotopic ^{26}Mg. Magnesium-26 enhancements are well correlated with ^{27}Al abundances. This is clear evidence for ^{26}Al decay with an initial $^{26}Al/^{27}Al$ ratio of ~0.78. The white outline indicates the area used for the calculation of $^{26}Al/^{27}Al$.

simply the result of different tuning conditions in the NanoSIMS between different laboratories but rather points to topography effects. We note that the two X grains from the literature with $^{26}Al/^{27}Al$ ratios of ~0.6 are particularly large, 9 μm for grain X4 from Amari et al. (1992) and 25 μm for "Bonanza" from Gyngard et al. (2018), so that a lower Al^+/Mg^+ sensitivity factor may be appropriate here. Unfortunately, no Al^+/Mg^+ sensitivity factors are published in both works. This and their large sizes make it difficult to decide whether true $^{26}Al/^{27}Al$ ratios might be larger than reported. For further discussion we will assume that the reported $^{26}Al/^{27}Al$ ratios represent the true ratios. But for some smaller X grains from the literature, reported $^{26}Al/^{27}Al$ ratios may be too low by a factor of ~2, which would add to the effect of potential Al contamination on too low inferred $^{26}Al/^{27}Al$ ratios of many X (and other types of presolar) grains.

Given the low level of Al contamination and the relatively well-constrained Al^+/Mg^+ sensitivity factor used here, the new X grains provide a good opportunity for a comprehensive comparison of multielement isotope data, including diagnostic ^{26}Al, with SN models from the literature. For this comparison we have considered 12 SN models, including both "classical" and H ingestion CCSN models. The first group comprises models from Rauscher et al. (2002; s1528c, s25a34d), Woosley & Heger (2007; s12a, s15a), and Limongi & Chieffi (2018; 015a000, 015a300, 025a000, 025a300). For the second group we consider models 25T-H, 25T-H5, 25T-H10, and 25T-H50 of Pignatari et al. (2015).

Rauscher et al. (2002) presented isotope yields for CCSNe with masses from 15 to 25 $M_\odot$ and solar metallicity after the passage of the shock wave but prior to the mixing of the ejecta. Before they explode, massive stars consist of concentric layers that experience different stages of nuclear burning. It was previously shown that selective, large-scale mixing of matter from different SN zones in the Rauscher et al. models could account for many isotopic signatures of presolar grains (e.g., Nittler et al. 2008; Hoppe et al. 2010; Lin et al. 2010). A well-recognized problem with these mixing schemes, however, is that predicted $^{26}Al/^{27}Al$ ratios are too low to match the highest $^{26}Al/^{27}Al$ ratios in X grains. This is illustrated in Figure 4 in which profiles of $^{12}C/^{13}C$ and $^{26}Al/^{27}Al$ are displayed for the 15 $M_\odot$ model s15a28c. High $^{26}Al/^{27}Al$ ratios are predicted for the Ni and He/N zones which experienced explosive Si-burning and an α-rich freezeout from nuclear statistical equilibrium (Ni), and H-burning (He/N), respectively. However, Al is very low in the interior Ni zone, contrary to X grains, which have Al concentrations at a level of per mill to percent, leaving only the He/N zone as a potential source of high $^{26}Al/^{27}Al$ in X grains. The highest $^{26}Al/^{27}Al$ ratio in the He/N zone of model s15a28c is 0.4, a factor of 1.5–2 lower than those of our X grains; an even larger discrepancy exists for the $^{12}C/^{13}C$ ratio in the He/N zone, which is too low by two orders of magnitude (Figure 4). From this it becomes clear that ^{12}C-rich matter from other zones must have contributed to the condensation sites of X grains, which lowers predicted $^{26}Al/^{27}Al$ ratios. If we try to match the C and N isotopic ratios of our X grains within a factor of ~2, and the $^{29}Si/^{28}S$ ratios within ~20% by selective large-scale mixing, predicted $^{26}Al/^{27}Al$ ratios are too low by factors of 20–40. Similar problems are encountered with the 25 $M_\odot$ model s25a34d of Rauscher et al. (2002) in which the He/N zone has a maximum $^{26}Al/^{27}Al$ ratio of 0.3.

Similar to Rauscher et al. (2002), Woosley & Heger (2007) presented isotope abundance data for a set of CCSN models with masses from 12 $M_\odot$ to 120 $M_\odot$ and solar metallicity. We have explored two of their models, model s12a for a 12 $M_\odot$ and model s15a for a 15 $M_\odot$ star. Both models behave similarly to the 15 $M_\odot$ model of Rauscher et al. (2002) with the highest $^{26}Al/^{27}Al$ ratios of 0.4 in the He/N zone. Another set of CCSN nucleosynthesis models was recently presented by Limongi &

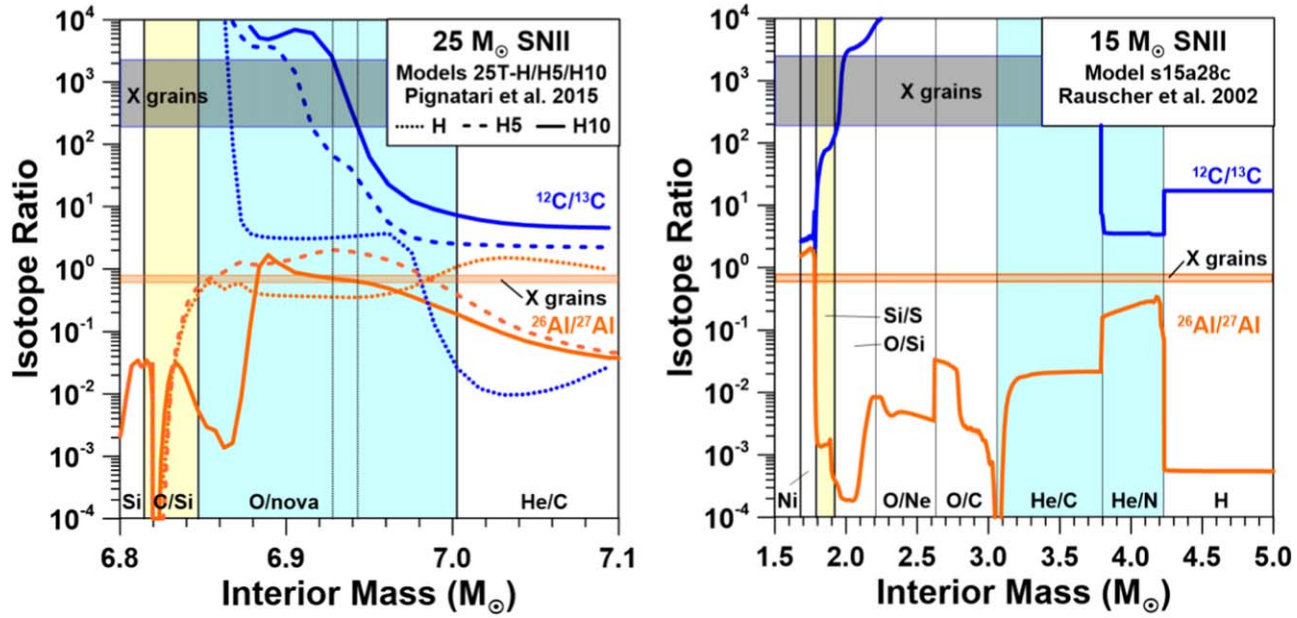

Figure 4. Left: profiles of $^{12}C/^{13}C$ and $^{26}Al/^{27}Al$ ratios in the interior of a 25 $M_\odot$ SN according to models 25T-H, 25T-H5, and 25T-H10 of Pignatari et al. (2015). The yellow and blue areas denote the C/Si and O/nova zones, respectively. Note that the Si zone (below the C/Si zone) provides lots of ^{28}Si, required to account for the isotopically light Si of X grains; other isotopic ratios are only marginally affected by the admixture of matter from this zone. The ranges of C and Al isotopic ratios of X grains with high initial $^{26}Al/^{27}Al$ ratios are indicated by horizontal bars. The two vertical dotted black lines represent the mass coordinates between which the ranges of C and Al isotopic compositions of X grains can be simultaneously reproduced by model 25T-H10 (see Figure 1). Right: profiles of $^{12}C/^{13}C$ and $^{26}Al/^{27}Al$ ratios in the interior of a 15 $M_\odot$ SN according to model s15a28c of Rauscher et al. (2002). The eight SN zones are named according to the most abundant elements in the respective zone. The ranges of C and Al isotopic ratios of X grains with high $^{26}Al/^{27}Al$ ratios are indicated by horizontal bars.

Chieffi (2018). This work considers stellar masses from 13 $M_\odot$ to 120 $M_\odot$, a range of metallicities, and different rotation velocities. We have explored their solar metallicity models 015a000 (15 $M_\odot$, no rotation), 015a300 (15 $M_\odot$, with rotation), 025a000 (25 $M_\odot$, no rotation), and 025a300 (25 $M_\odot$, with rotation). Maximum $^{26}Al/^{27}Al$ ratios are between 0.04 and 0.1, i.e., even lower than in the Rauscher et al. (2002) and Woosley & Heger (2007) models.

As we have shown above, the high $^{26}Al/^{27}Al$ ratios of 0.6-0.8 as observed in the X grains presented here and in two X grains from the literature cannot be explained in the context of "classical" SN models. In the following we will focus on the H ingestion SN models presented by Pignatari et al. (2015) and Schofield et al. (2022). These authors provide isotope data for a set of 25 $M_\odot$ CCSNe of solar metallicity that experienced H ingestion into the He shell prior to the explosion. Compared to the original 25 $M_\odot$ stellar simulations (Pignatari et al. 2016), these models use an artificially increased temperature and density in the He shell to mimic the temperature and density evolution of a 15 $M_\odot$ SN during the explosion. Explosive H- and He-burning occur at the bottom of the He shell during the passage of the SN shock, leaving characteristic isotopic and elemental signatures in the He shell. The He shell ejecta can be divided into three distinct zones: a thin (<0.04 $M_\odot$) C/Si zone at the bottom, and the O/nova and He/C zones above (Figure 4). Here, we explored models 25T-H, 25T-H5, 25T-H10, and 25T-H50. Model 25T-H considers an H concentration of 1.2% in the He shell, model 25T-H5 0.24%, model 25T-H10 0.12%, and model 25T-H50 0.024%. While model 25T-H50 shows similarly low $^{26}Al/^{27}Al$ ratios as the classical SN models, much higher ratios of up to ~2 are predicted for the O/nova or He/C zones in models 25T-H, 25T-H5, and 25T-H10 (Figure 4). Model 25T-H10 is particularly promising as it (i) provides a thin layer around 6.94 $M_\odot$ in which the ranges of $^{12}C/^{13}C$ and $^{26}Al/^{27}Al$ ratios of X grains with high $^{26}Al/^{27}Al$ ratios can be simultaneously well matched (Figures 1, 4; note that the match is worse for models 25T-H and 25T-H5) and as it (ii) provided a good match of multielement isotope data of X grains discussed in Hoppe et al. (2018). When we consider mixing over larger scales, namely, 0.2–0.4 $M_\odot$, considering matter from the Si, C/Si, O/nova, and He/C zones (see Figure 4), and a C-N fractionation factor of 50 during condensation (Hoppe et al. 2018) it is possible to match all measured isotope ratios ($^{12}C/^{13}C$, $^{14}N/^{15}N$, $^{26}Al/^{27}Al$, $^{29,30,32}Si/^{28}Si$) of our six X grains by model 25T-H10 reasonably well; for $^{12}C/^{13}C$ within 30%, for $^{14}N/^{15}N$ within a factor of 3, for $^{26}Al/^{27}Al$ within 15%, for $^{29}Si/^{28}Si$ within 20%, for $^{30}Si/^{28}Si$ within a factor of 2, and for $^{32}Si/^{28}Si$ within a factor of 3. Carbon/O ratios are <1 for these mixtures. This is a well-known problem when X grain isotope data are fitted in the context of H ingestion SN models (e.g., Hoppe et al. 2018) and deserves further attention in future studies. Under thermodynamic equilibrium conditions SiC formation requires C/O > 1 (Lodders & Fegley 1992). Clayton et al. (1999) suggested condensation of carbonaceous grains while C/O < 1 in CCSN ejecta, which, however, was questioned for SiC (Ebel & Grossman 2001).

The H ingestion SN models are still uncertain in several aspects (Pignatari et al. 2015; Clarkson & Herwig 2021; Schofield et al. 2022). For instance, the effective size of the O/nova zone will depend on the SN shock energy when the He shell layers are reached (Pignatari et al. 2015; Schofield et al. 2022), as well as on the progenitor structure of the same layers. Here, the impact of the H ingestion event is expected to leave remarkable signatures that cannot be predicted by one-dimensional models (Herwig et al. 2014; Woodward et al. 2015). These effects will have an important impact on how the SN shock energy will be converted to a temperature and

density peak. Interestingly, we have seen that a maximum value of $^{26}Al/^{27}Al$ of ∼2 is reached for a range of H concentrations between 1% and 1 per mill (Figure 4). Such a ratio is the product of the combination of explosive H-burning in conditions more typical of explosive He-burning, and of the nuclear reaction rates activated. The $^{26}Al/^{27}Al$ ratios of X grains can be used in the future in evolved SN models to directly constrain (i) the local conditions of the He shell right after the H ingestion, (ii) the range of shock conditions experienced by the parent SNe, and (iii) the amount of material condensed in grains coming from the ^{26}Al-rich parts of He shell layers.

As we have shown in this Letter, the high $^{26}Al/^{27}Al$ ratios of 0.6-0.8 of all SiC X grains reported here favor the scenario where they have been formed in the ejecta of CCSNe whose stellar progenitors were affected by significant H ingestion events, leaving still unburnt H in the He shell layers. It is hoped that our new and diagnostic Al isotope data of X grains will motivate the development of H ingestion SN models further, which should include three-dimensional hydrodynamics and consistent calculations of explosive conditions generated by the stellar progenitor.

We thank Antje Sorowka for SEM analyses, Elmar Gröner and Philipp Schuhmann for technical support on the Nano-SIMS, Alexander Heger and Alessandro Chieffi for providing detailed SN data, and an anonymous referee for constructive and helpful comments. MP thanks the ERC Consolidator Grant (Hungary) Program (RADIOSTAR, G.A. n. 724560), the STFC (through the University of Hull's Consolidated Grant ST/R000840/1), the ChETEC COST Action (CA16117), supported by the European Cooperation in Science and Technology, the ChETEC-INFRA project funded by the European Union's Horizon 2020 research and innovation program under grant agreement no. 101008324, and the US IReNA Accelnet network (Grant No. OISE-1927130). MP also acknowledges the support to NuGrid from JINA-CEE (NSF Grant PHY-1430152), the ongoing access to Viper, the University of Hull High Performance Computing Facility, and the "Lendület-2014" program of the Hungarian Academy of Sciences.

ORCID iDs

Peter Hoppe https://orcid.org/0000-0003-3681-050X
Jan Leitner https://orcid.org/0000-0003-3655-6273
Marco Pignatari https://orcid.org/0000-0002-9048-6010
Sachiko Amari https://orcid.org/0000-0003-4899-0974

References

Amari, S., Hoppe, P., Zinner, E., & Lewis, R. S. 1992, ApJL, 394, L43
Amari, S., Lewis, R. S., & Anders, E. 1994, GeCoA, 58, 459
Bernatowicz, T., Fraundorf, G., Ming, T., et al. 1987, Natur, 330, 728
Besmehn, A., & Hoppe, P. 2003, GeCoA, 67, 4693
Clarkson, O., & Herwig, F. 2021, MNRS, 500, 2685
Clayton, D. D., Liu, W., & Dalgarno, A. 1999, Sci, 283, 1290
Ebel, D. S., & Grossman, L. 2001, GeCoA, 65, 469
Groopman, E., Zinner, E., Amari, S., et al. 2015, ApJ, 809, 31
Gyngard, F., Jadhav, M., Nittler, L. R., Stroud, R. M., & Zinner, E. 2018, GeCoA, 221, 60
Gyngard, F., Nittler, L. R., & Zinner, E. 2010, M&PS, 45, A72
Herwig, F., Woodward, P. R., Lin, P.-H., Knox, M., & Fryer, C. 2014, ApJL, 792, L3
Hoppe, P., Fujiya, W., & Zinner, E. 2012, ApJL, 745, L26
Hoppe, P., Leitner, J., Gröner, E., et al. 2010, ApJ, 719, 1370
Hoppe, P., Pignatari, M., Kodolányi, J., Gröner, E., & Amari, S. 2018, GeCoA, 221, 182
Hoppe, P., Stancliffe, R. J., Pignatari, M., & Amari, S. 2019, ApJ, 887, 8
Hoppe, P., Strebel, R., Eberhardt, P., Amari, S., & Lewis, R. S. 1996, Sci, 272, 1314
Hoppe, P., Strebel, R., Eberhardt, P., Amari, S., & Lewis, R. S. 2000, M&PS, 35, 1157
Lewis, R. S., Amari, S., & Anders, E. 1994, GeCoA, 58, 471
Limongi, M., & Chieffi, A. 2018, ApJS, 237, 13
Lin, Y., Amari, S., & Pravdivtseva, O. 2002, ApJ, 575, 257
Lin, Y., Gyngard, F., & Zinner, E. 2010, ApJ, 709, 1157
Liu, N., Barosch, J., Nittler, L. R., et al. 2021, ApJL, 920, L26
Liu, N., Nittler, L. R., Alexander, C. M. O. D., & Wang, J. 2018, SciA, 4, eaao1054
Liu, N., Nittler, L. R., Pignatari, M., Alexander, C. M. O. D., & Wang, J. 2017, ApJL, 842, L1
Lodders, K., & Fegley, B., Jr. 1992, Metic, 27, 250
Lugaro, M., Davis, A. M., Gallino, R., et al. 2003, ApJ, 593, 486
Lugaro, M., Karakas, A. I., Pető, M., & Plachy, E. 2018, GeCoA, 221, 6
Marty, B., Chaussidon, M., Wiens, R. C., Jurewicz, J. G., & Burnett, D. S. 2011, Sci, 332, 1533
Nittler, L. R., & Alexander, C. M. O. D. 2003, GeCoA, 67, 4961
Nittler, L. R., Alexander, C. M. O. D., Gallino, R., Hoppe, P., et al. 2008, ApJ, 682, 1450
Nittler, L. R., Amari, S., Zinner, E., Woosley, S. E., & Lewis, R. S. 1996, ApJL, 462, L31
Nittler, L. R., & Ciesla, F. 2016, ARA&A, 54, 53
Nittler, L. R., & Hoppe, P. 2005, ApJL, 631, L89
Palmerini, S., Busso, M., Vescovi, D., et al. 2021, ApJ, 921, 7
Pignatari, M., Herwig, F., Hirschi, R., et al. 2016, ApJS, 225, 24
Pignatari, M., Zinner, E., Bertolli, M. G., et al. 2013, ApJL, 771, L7
Pignatari, M., Zinner, E., Hoppe, P., et al. 2015, ApJL, 808, L43
Rauscher, T., Heger, A., Hoffman, R. D., & Woosley, S. E. 2002, ApJ, 576, 323
Schofield, J., Pignatari, M., Stancliffe, R. J., & Hoppe, P. 2022, MNRAS, 517, 1803
Stephan, T., Bose, M., Boujibar, A., et al. 2021, in LII Lunar and Planetary Science Conf. (Houston, TX: Lunar and Planetary Institute), Abstract #2358
Woodward, P. R., Herwig, F., & Lin, P.-H. 2015, ApJ, 798, 49
Woosley, S. E., & Heger, A. 2007, PhR, 442, 269
Xu, Y., Zinner, E., Gallino, R., et al. 2015, ApJ, 799, 156
Zinner, E. 2014, in Meteorites and Cosmochemical Processes, ed. A. M. Davis (Amsterdam: Elsevier), 181